The gradual phase of the X17 flare on October 28 2003

G. Del Zanna
MSSL, University College London Holmbury St. Mary Dorking RH5 6NT UK

B. Schmieder
Observatoire de Paris, Section de Meudon, LESIA, F-92195 Meudon Principal Cedex, France

H. Mason
DAMTP, Centre for Mathematical Sciences, University of Cambridge, Wilberforce Road, Cambridge CB3 0WA, UK

A. Berlicki
Wroclav Observatory, Poland

S. Bradshaw
Space and Atmospheric Physics, Blackett Laboratory, Imperial College London, Prince Consort Road, London, SW7 2BZ, UK

March 24, 2006

Abstract.

In this paper, we present SOHO/CDS observations taken during the gradual phase of the X17 flare which occurred on October 28, 2003. The CDS data are supplemented with TRACE and ground-based observations. The spectral observations allow us to determine velocities from the Doppler-shifts measured in the flare loops and in the two ribbon kernels, one hour and half after the flare peak. Strong downflows ($>$ 70 km/s) are observed along the loop legs at transition region temperatures. The velocities are close to those expected for free fall. Observations and results from a hydrodynamic simulation are consistent with the heating taking place for a short time near the top of the arcade. Slight up-flows are observed in the outer edges of the ribbons ($<$ 60 km/s) in the EUV lines formed at log T $<$6.3. These flows could correspond to the so-called "gentle evaporation". At 'flare' temperatures (Fe XIX, logT=6.9), no appreciable flows are observed. The observations are consistent with the general standard reconnection models for two-ribbons flares.

Keywords: solar flares, EUV lines

1. Introduction

On October 28 2003 at 11:02 UT, AR 10486 unleashed one of the biggest solar flares (class X17) ever recorded. This event, observed with many instruments, was complex and presented various phases. After a few smaller flares, various filament eruptions and the main X17 X-ray flare, a multiple-ribbon structure and an arcade of loops formed. Various studies of this event have been published (Zhang et al. 2003, Régnier and Fleck 2004, Schmieder et al. 2005). Here, we focus only

on the gradual phase and present an analysis of the flows observed in these structures in EUV lines.

At first glance, the overall morphology of this event fits the standard picture of a two-ribbon flare, in which arcades of 'cool' loops (observed in Hα) and in 'hot' loops (as seen e.g. in 195 Å or 171 Å with EIT and TRACE and with Yohkoh SXT) are observed to continuously form and expand. The footpoints of these loops are normally well observed in Hα and EUV lines and form the ribbons. During the formation of the loops, the ribbons separate at high speeds (see, e.g., Fletcher & Hudson 2001, Asai et al. 2002). Hα and X-ray observations (e.g. Yohkoh SXT) have often shown that the hotter loops are located above the cooler Hα loops (see e.g. Schmieder et al 1995). The density of the Hα loops is often estimated to be relatively high, decreasing from 10^{11} cm^{-3} to 10^{10} cm^{-3} over time. The densities in the hotter loops are thought to be lower than the cool loop densities (Schmieder et al 1996). The plasma in the Hα loops has often been observed to flow down the legs at speeds which can reach the free fall (50 to 150 km/s) (Wiik et al. 1996).

These types of observations have suggested standard models- 'the CSHPK model' of reconnection of open magnetic field lines in the corona (Kopp and Pneuman 1976, Kopp and Poletto 1984, Forbes and Malherbe 1986, Forbes and Acton 1996). The reconnection of the open field lines occurs at a magnetic X-line which moves upward as the region of closed loops grows. The loops and ribbons are associated with the field lines which map from the X-line to the chromosphere.

The reconnection process naturally explains the existence of high temperatures in hot loops. Thermal condensation (cf. Antiochos and Sturrock 1978) could form the cool loops from the hot loops. Another important process is the evaporation of material that fills the hot loops. For our understanding of flares, it is important to study the role of the mechanisms that replenish/empty the loops (free fall, evaporation and condensation), as well as the processes that create the ribbons (thermal conduction, bremsstrahlung of energetic particles).

One of the limitations in testing the different processes has been a lack of spectroscopic measurements that could cover a broad range of temperatures. Doppler-shift measurements in a broad band of temperatures should be a good diagnostic of processes at work during a flare. Many earlier observations have been performed with the Skylab and SMM instruments, but there were limitations in either spatial or spectral capability. In the past decade, SOHO has has given us the opportunity to study solar flares in more detail, in particular with the Coronal Diagnostic Spectrometer (CDS) and SUMER instruments.

Given the limited field of view (max 4'x4'), sensitivity and telemetry constraints, CDS observations of flares are relatively infrequent. The

first SOHO/CDS measurements of a two-ribbon flare were reported in a *letter* by Czaykowska et al (1999). These authors reported SOHO/CDS observations of an arcade of hot loops two hours after the peak of an M6.8 flare. Blue-shifts in Fe XVI (3×10^6 K) and Fe XIX (8×10^6 K) lines appeared to be located at the outer edges of the flare ribbons. Similar observations were reported by Harra et al. (2005).

Spatially-resolved spectral information from CDS were reported by Del Zanna et al (2002) covering the entire evolution of a small flare. Long lasting (over an hour) blue-shifts of 30 km/s in coronal lines (Mg X, Si XII, emitted at 1-2 MK) were located at the footpoints of a small loop system.

Recent results seem to provide a more complex description of the phenomena. It seems to be difficult to separate the different evolution phases of a flare. Del Zanna et al. (2006) found strong blue-shifts in CDS coronal lines in some flare kernels during the impulsive phase (with velocities increasing with the line formation temperature), but no flows at all in some other kernels for the same flare. Kamio et al. (2003) also observed down-flows over the flare ribbons in Hα line and weak velocities in O V with CDS. Li et al. (2005) observed down-flows in Hα and Ca II lines throughout their observations (20 min.) which is too long to represent only the impulsive phase. Their observation suggest that reconnection is still continuing during the gradual phase, non-thermal electrons are still produced and bombard the chromosphere. Condensation of chromospheric plasma and explosive evaporation are still expected.

In this paper we present the observations of post-flare loops and ribbons observed one hour and half after the X17 flare of October 28 2003. In section 2 we describe the observations with SOHO/CDS and TRACE. In section 3 we present the flows measured by analyzing the CDS line profiles. In section 4 we discuss the results in the context of the magneto-hydrodynamical models.

2. CDS and TRACE Observations

On October 28 2003 we had coordinated a multi-wavelength campaign of observations on AR 10486. SOHO/CDS performed various scans of the active region before and during the flare. Here we present results from one fast (20 minutes) NIS raster, that we designed to cover a wide range of temperatures (He I 584 Å, log T =4.5; O IV 625.9 Å, log T = 5.3; O V 630 Å, log T = 5.4; Mg X 625 Å, log T = 6.0; Si XII 520.8 Å, log T = 6.3; Fe XIX 592.2 Å, log T = 6.9), and to provide electron densities. This NIS raster observed the active region during the gradual

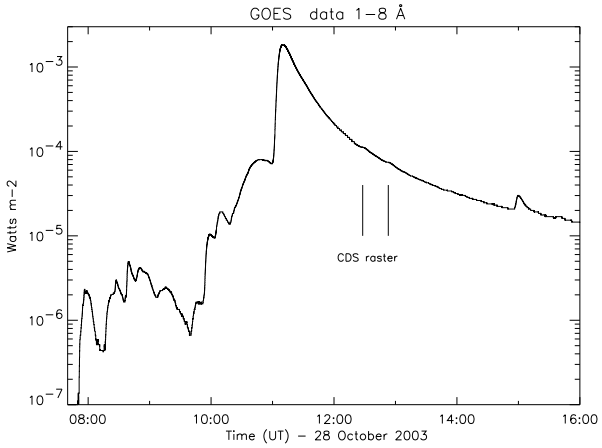

Figure 1. Evolution of the GOES X-ray fluxes during the October 28, 2003 X17 flare, with the timing of the CDS raster.

phase (12:28-12:52 UT, see Fig. 1). TRACE recorded images in the 195 and 1600 Å bands with a cadence of 30-40 s.

The TRACE images alone cannot provide an accurate map of the temperature structure of the flare. The TRACE 195 Å band is in fact multi-thermal, with varying contributions from transition region (Fe VIII), coronal (e.g. Fe XII) and flare (e.g. Fe XXIV) plasmas. The interpretation of the TRACE images in the 1600 Å band is also non-trivial. The CDS monochromatic images, despite having a much lower spatial (6" against 1" of TRACE) and temporal resolution can provide important information.

CDS/NIS does not observe Fe XXIV emission, however the Fe XIX 592.2 Å line can be used as a proxy to estimate which parts in the TRACE 195 Å images are the hottest. Wherever Fe XIX emission is strong, we expect a strong contribution to the TRACE band by flare lines.

The Hα images (see Fig. 2) show the locations of the ribbons. The TRACE 1600 Å images (dominated by UV continuum and neutral ion emissions) also clearly indicate the presence of a multiple ribbon structure. The two main ribbons R1 (positive) and R2 (negative) (cf. Fig. 2) are located above the main sunspots of opposite polarity. In the TRACE 195 Å band, an arcade of loops that connect the two ribbons R1 and R2 is visible. A sample of TRACE images taken during the CDS scan are shown in Fig. 3, together with the locations of the CDS slit as a function of time. The CDS scans normally from west to east. Two portions of the flaring area are shown in Figs. 5,8.

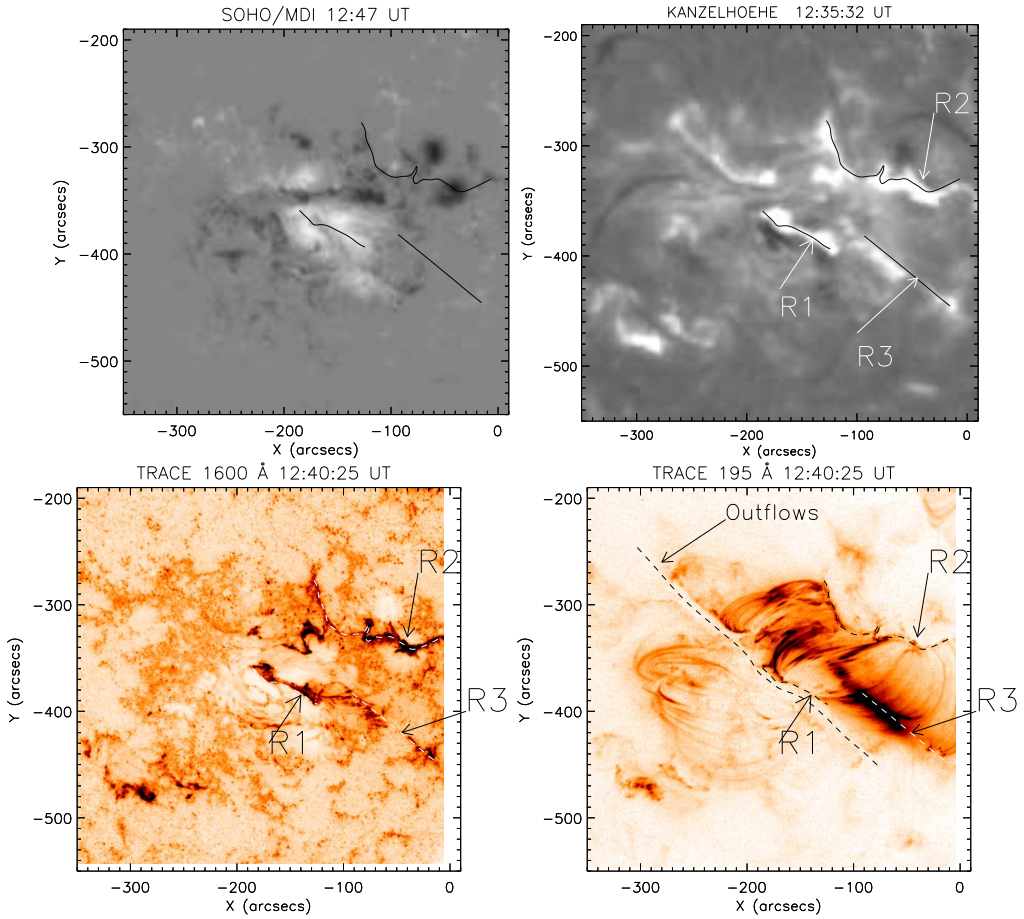

Figure 2. From top to bottom and left to right: SOHO/MDI magnetogram; Hα image obtained during the CDS raster; TRACE 1600, 195 Å images (negative). Note the similarities between the TRACE 1600 Å and the Hα images. Notice the arcade of loops seen in TRACE 195 Å connecting the ribbon structures R1, R2 which are located above the sunspot regions of opposite polarity. Also note the system of loops in TRACE 195 Å which connects R3 to R1 and R2. R3 is seen in TRACE 1600 Å as an almost straight line of emission. The central part of R3 is also the location of the strongest emission in TRACE 195 Å.

The upper part of the flare region shows rising loops (nos. 1,2 in Fig. 5) with apparent unidirectional flows. The central part of the arcade, connecting R1 and R2, shows condensations along loops (cf. no. 3 in Fig. 5) that appear and disappear in the TRACE 195 Å band over the imaging cadence (30-40 s). Some brightenings appear to flow from the top of the central part of the arcade toward the two main ribbons R1 and R2. During the CDS scan (20 min.), the ribbons R1 and R2 separate by just a few arcseconds, while the arcade slowly rises in

height. All this fits the standard CSHPK model. Notice that during the CDS scan the main features persisted, and the location of the ribbons, at the CDS resolution, can be considered as stationary. Therefore CDS observations enable us to study some general properties of this gradual phase.

CDS data (see Fig. 10) indicate that most of the hottest emission in the central arcade connecting R1 and R2 is located in the central area. However, significant Fe XIX emission is also present all along the loops, as is emission from lines formed at lower temperatures.

As shown in Figs. 2,3,8, a third structure (R3) is seen in the TRACE 1600 Å and Hα images as an almost straight line of emission, overlying a region of weak fields. The brightest TRACE 195 Å emission is co-located with R3. The central part is much less variable than the other regions, and brightenings in both 195 and 1600 Å bands flow only from R3 toward R1.

The CDS observations clearly show that the peak emission in Fe XIX is co-spatial with the strongest emission in the TRACE 195 Å band (top part of R3 - the lower parts were not observed). This suggests that the hottest emission in the entire region is concentrated in R3.

One obvious interpretation would be that R3 represents in projection both the top of Hα and coronal loops. In one case (loop 5 in Fig. 8) it is possible to trace a long tilted structure that connects R1 with R2. However, this does not explain why downflows appear to only occur on one side. Also, most structures appear to be connected between R3 and R2 and appear relatively stationary.

A more likely explanation is that R3 represent a filament. Indeed R3 is approximately in the location where a filament eruption previously occurred. It is relatively common to observe filaments in emission at different wavelengths. It would not be the first time that 10 MK emission is observed in the same locations where Hα emission is present (cf. Del Zanna et al. 2006). However, this normally occurs during the initial phase of a flare.

To complicate further projection effects, there are a few loops (cf. 7,8,9 in Fig. 8) that connect R2 with magnetic concentrations of positive polarity, almost aligned with R3 (see Fig. 9).

3. Flows and density

CDS does not have an abolute wavelength scale (see details in Del Zanna et al. 2006) so we have taken an area outside the flare and considered the averaged wavelengths as the rest values. We have neglected the small deviations (of the order of 5 km/s) that would be present in

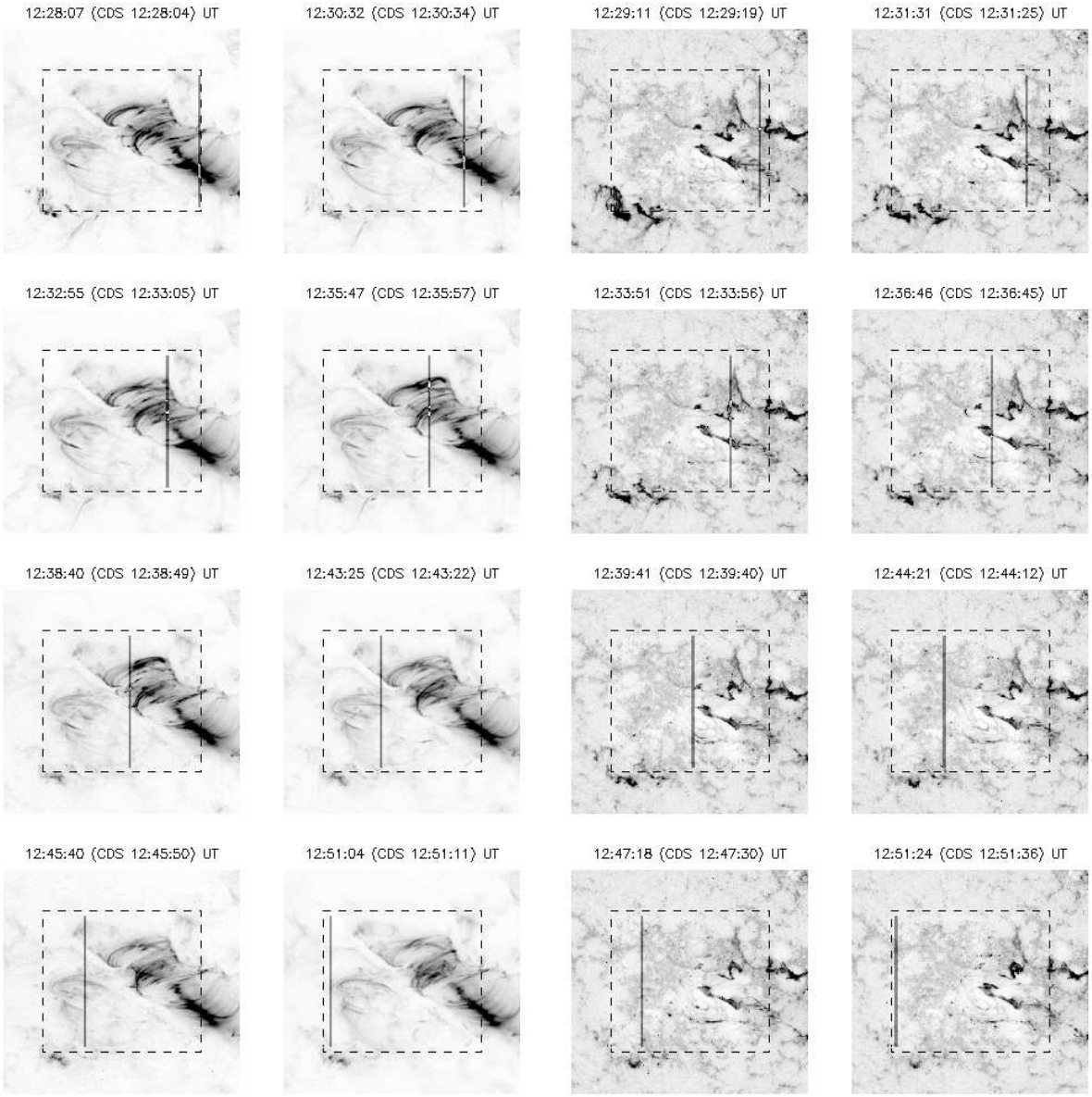

Figure 3. Sequence of TRACE 195 (left), 1600 (right) Å images taken during the CDS raster, shown with the same intensity scale. The FOV of the CDS raster, and the position of the slit as a function of time are shown. Note that overall the loop structures seen in TRACE 195 Å and the ribbon structures seen in TRACE 1600 Å remain largely unchanged.

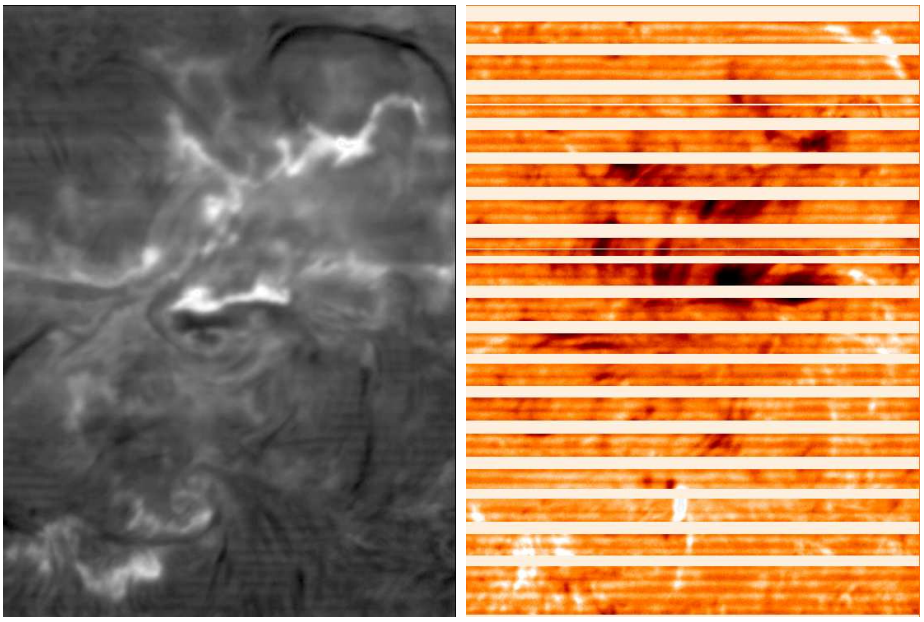

Figure 4. Intensity in the Hα line centre (left image) and Dopplergram of the active region in Hα +/- 0.8 Å(right image) obtained at the Wroclaw (Bialkov) observatory with the MSDP spectrograph at 12:40:59 UT. Note the location of the ribbons in the intensity image. Dark areas in the Dopplergram image indicate strong ($v > 100$ km/s) downflows. The stripes are due to missing signal in the Hα wings. (see for details the text in section 3).

Table I. Results from the averaged spectra of the various regions displayed in Fig. 11. For each of the selected spectral lines, we display the averaged velocities v (in km/s; negative corresponds to blue-shift), and the calibrated line intensities I (erg cm^{-2} s^{-1} sr^{-1}). Averaged electron densities N_e (10^{10} cm^{-3}) were obtained from O IV line ratios.

Region	O1	O2	R1a	R1b	R3	R2a	R2b	R2c
He I v	-31	-28	35	4	47	65	47	13
I	98	126	2190	259	838	1090	1040	588
N_e (O IV)	-	0.6±0.3	3.3±1.4	-	1±0.4	0.6±0.3	1.3±0.8	1.7±0.8
O V v	-17.	-25	72	35	70	64	55	6
I	1340	2870	16300	2040	5350	6222	15000	4240
Mg X v	-61.	-56	37	-4	17	23	22	-9
I	262	333	7290	296	1850	2940	4820	1080
Si XII v	-62	-28	25	-18	13	28	12	-13
I	203	274	8070	281	1810	4290	6460	1500
Fe XIX v	-	-	5	-45	3	14	0	-27
I	-	-	2290	75	1320	1210	1333	444

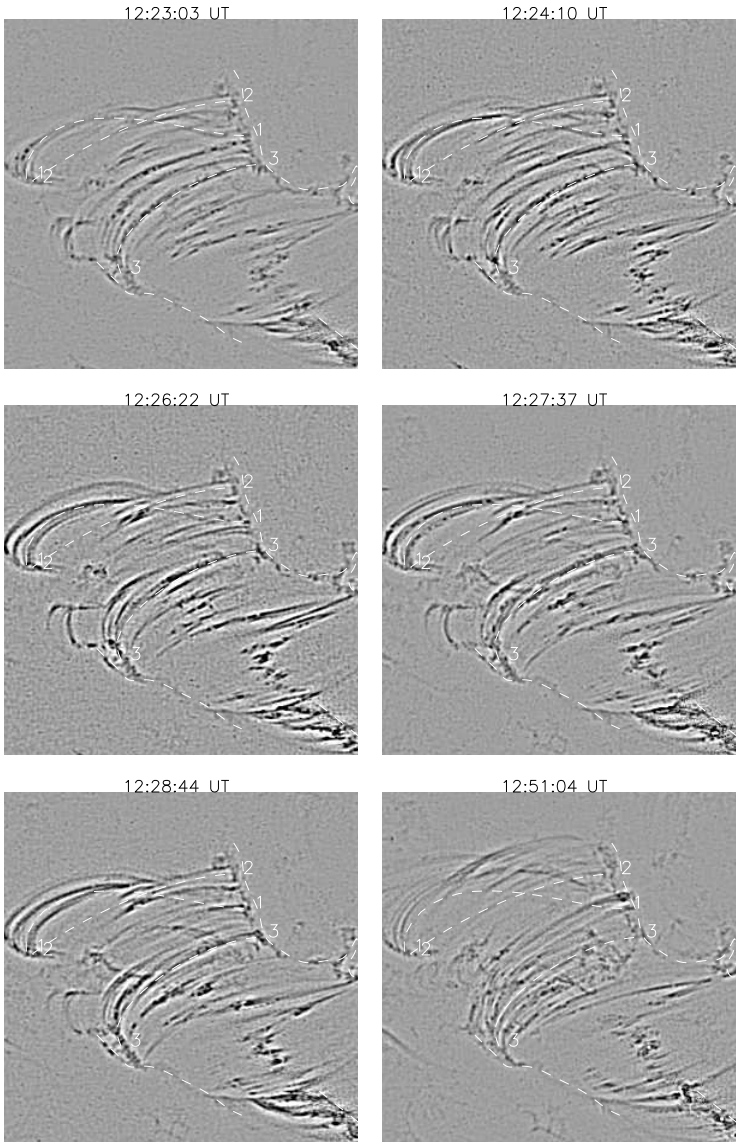

Figure 5. Sequence of TRACE 195 images (enhanced by subtracting a smoothed image) taken during the CDS raster, with superimposed a few loop structures and the locations of R1, R2, R3 (see text).

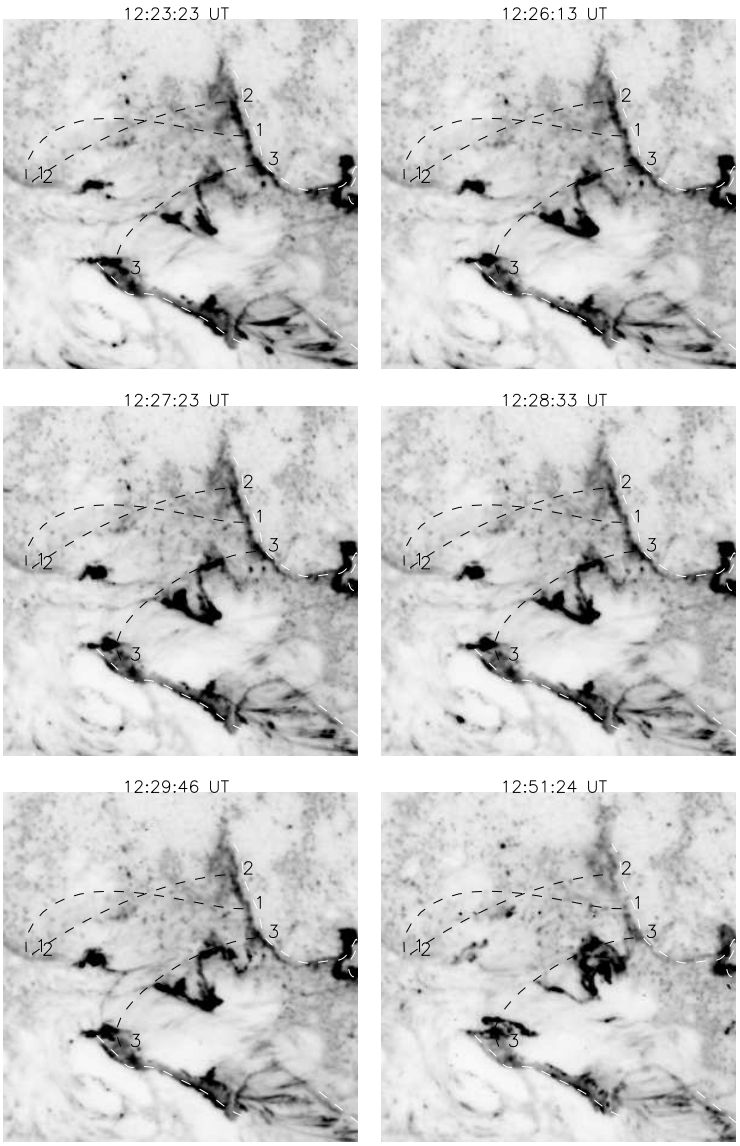

Figure 6. Sequence of TRACE 1600 Å negative images taken during the CDS raster, with a few loops superimposed (marked by numbers at their footpoints), and the locations of R1, R2, R3 (see text).

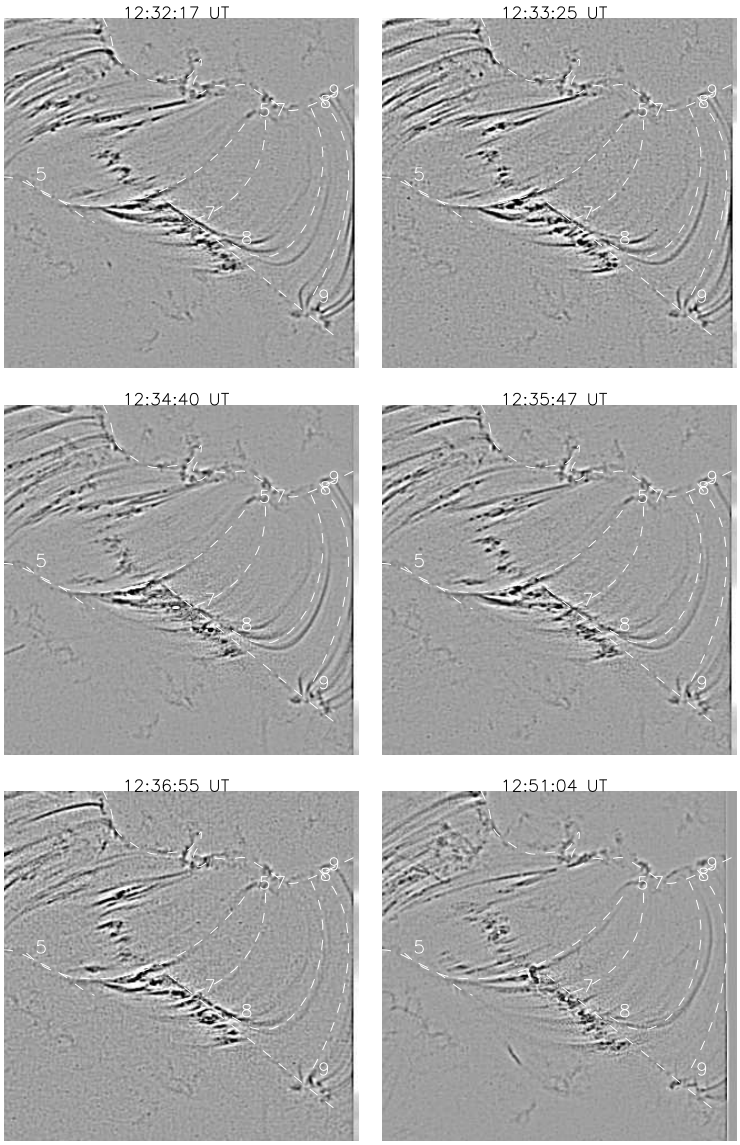

Figure 7. Sequence of TRACE 195 images (enhanced) taken during the CDS raster, with superimposed a few loop structures and the locations of R1, R2, R3 (see text).

some transition region lines, and are due to the overall redshifts present in these lines. This is because uncertainties in the measurements of line positions are larger (about 10 km/s). The coarse spectral resolution of CDS does not allow a simultaneous fit of a rest and a red- or blue-shifted component, so we have fitted the CDS lines with single components, to identify the main flows.

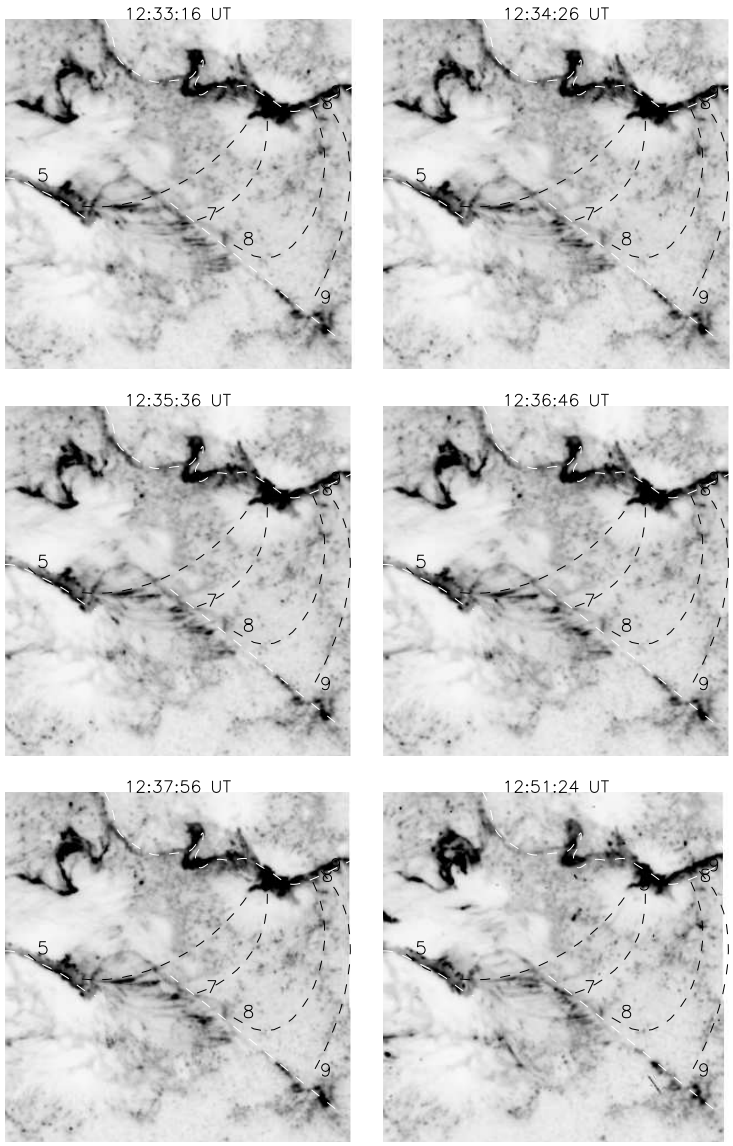

Figure 8. Sequence of TRACE 1600 Å negative images taken during the CDS raster, with a few loops superimposed (marked by numbers at their footpoints), and the locations of R1, R2, R3 (see text).

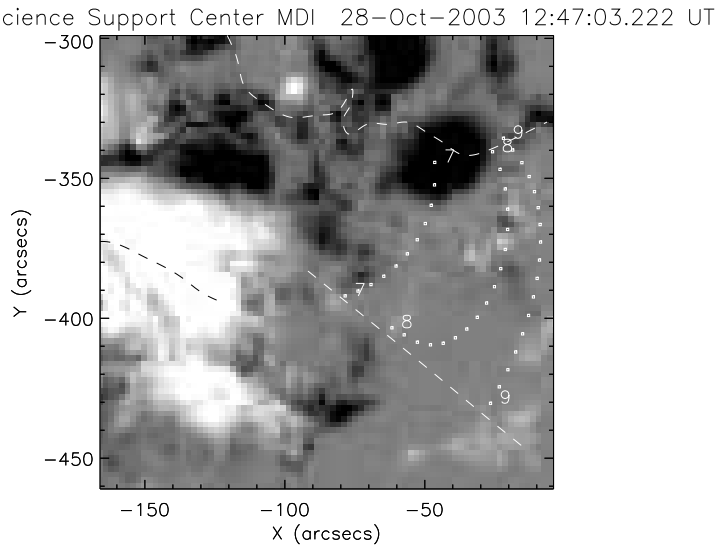

Figure 9. SOHO/MDI magnetogram with superimposed a few loop structures and the locations of R1, R2, R3. Loop structures such as nos. 7,8,9 connect polarities near the ribbon R2 with fragments located near the structure R3 (see text).

The CDS data show strong downflows near the R1,R2 kernels in all the transition region and coronal lines (see Fig. 10), which confirm the apparent motion seen with TRACE.

In order to increase the S/N, we have selected different regions (shown in Figure 11) to obtain averaged spectra and line parameters. The results of the computations are presented in Table I.

Strong down-flows ($v \simeq 70$ km/s) at transition region temperatures are observed in O V along the legs of the loops, which are located close to the inner edges of ribbons (R1a, R2a, R2b, R3). The velocity is decreasing as the temperature of the line formation increases. The flows in Fe XIX are nearly zero. These flows are close to the free fall velocity. The free fall velocity depends on the gas pressure height in the loops:
at 10^6 K, H=50 000 km then v=0
at 10^5 K, H=5 000 km then v$\simeq$10 km/s
at 10^4 K, H=500 km then v$\simeq$100 km/s.

Moderate upflows in all TR (e.g. OV) and coronal lines (e.g. Mg X) are observed in some localised regions outside the R1 and R2 ribbons, while strong upflows are located all along a region just outside R1,

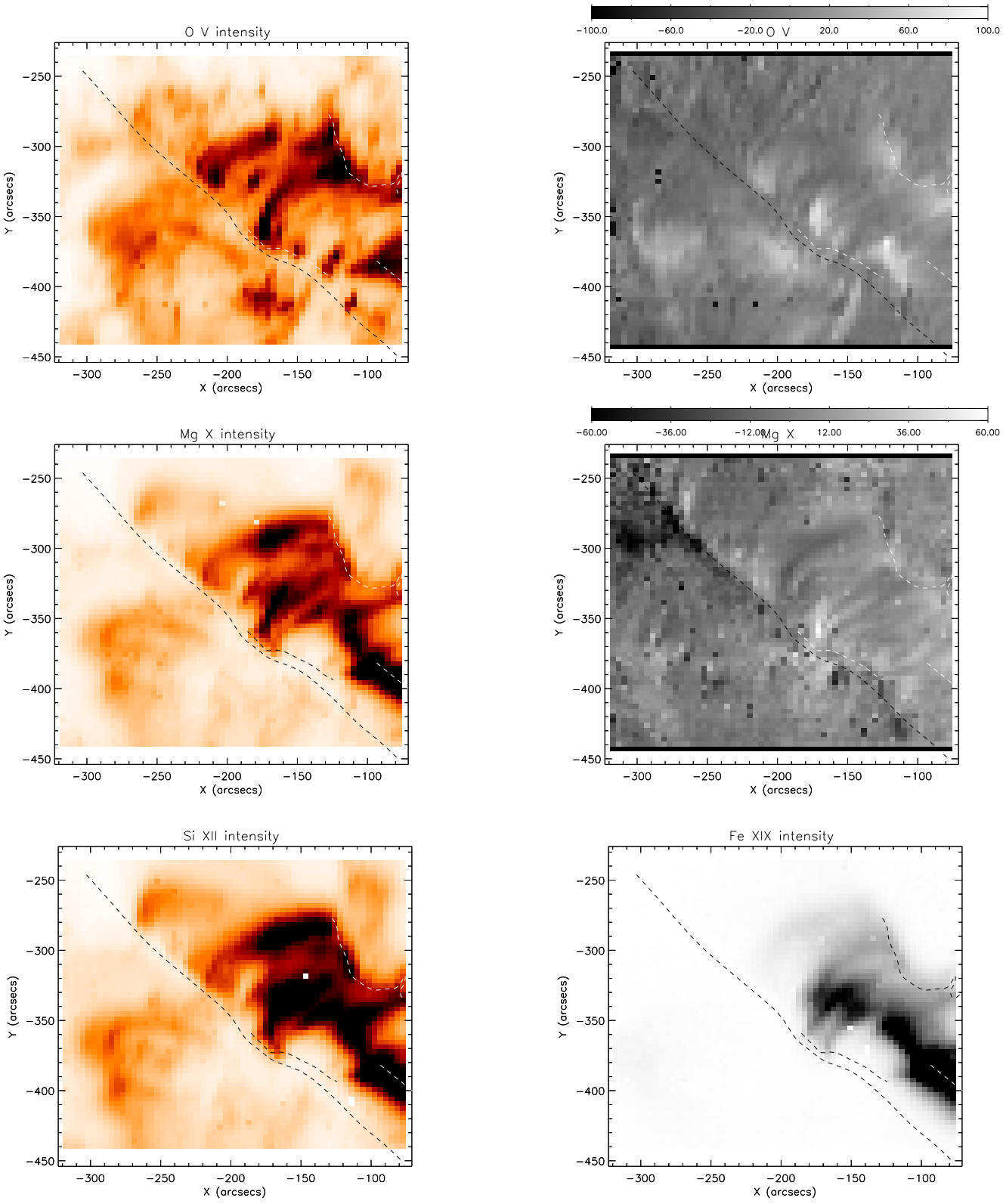

Figure 10. From top to bottom: CDS intensity and velocity maps in O V, Mg X; intensity maps in Si XII and Fe XIX. Strong downflows ($v \simeq 50 - 100$ km/s) near the ribbons are observed. The structures indicated in Fig.2 are superimposed.

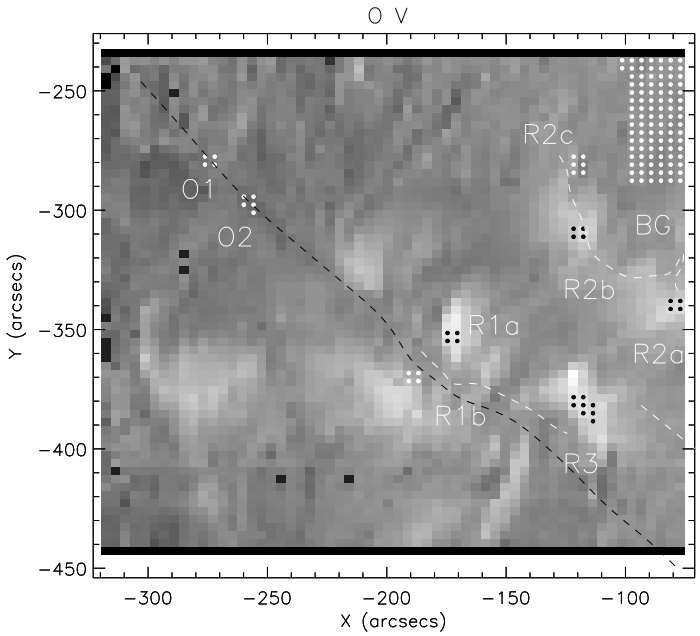

Figure 11. O V velocity map, with the few selected areas

coincident with a region of low emission in the TRACE 195 Å band (marked 'Outflow' in Fig. 2).

Moderate up-flows (< 30 km/s) in all the transition region lines (e.g. OV) and larger up-flows ($\simeq 60$ km/s) in coronal lines (e.g. Mg X) are observed. No significant velocity is observed in FeXIX lines. No similar region was ofind outside R2.

All the above flows correspond to averaged Doppler-shifts and should be considered as lower values to the real ones, due to the coarse spatial and spectral resolution of CDS, and the fact that the loop structure and the projection effects have not been taken into account.

In relation to the velocities of cool plasma observed in Hα, we computed Doppler-shift maps using the Multichannel Double Pass Spectrograph(MSDP) observations obtained at the Astronomocal Institute of the Wrocław University in Bialkow. Many observatories observed the development of this two ribbon flare with survey telescopes, in Asia, in Europe. Few of them have spectrographs which allow us to derive Dopplershifts. The MSDP spectrograph of Wrocław is a spectrograph with an open slit covering 30 $\times$ 100 arcsec and by selecting a thin wavelength band pass (0.250 A) we obtain a spectrum (along x the wavelength is varying and also the position on the sun). The observa-

tionof the active region is obtained by moving the large slit over the sun and an image by adding many elementary field-of-views. At the edges of each elementary field-of-view only half of the profile is observed. The Dopplershifts being derived with a bisector method and the spectral range of the MSDP is only 2 Å Doppler-shifts in the far wing of the Hα line cannot be computed. Therefore the large stripes are observed in Fig. 4. The dark areas in this image represent high downflows.

On the other hand, the Hα spectra of Ondrejov indicate that the velocities of the legs of the postflare loops are much larger than what we computed with the MSDP. They are certainly larger than 100 km/s.

Nevertheless to get a good estimate of the velocity a non-LTE radiative transfer modelling is necessary (see, e.g., Berlicki et al 2005) because the Hα line is optically thick. The background is also a very sensitive parameter in this kind of computation. In our case, we have sunspots as the main background. So, the background has to be carefully modelled before computing any velocity.

Densities could only be obtained using CDS O IV lines, in regions close to the legs of the arcade. We have recently revised the CHIANTI model for this ion (version 5.2) and obtained densities using the ratio of the 625.8 Å line vs. the multiplet observed at 554 Å. We found relatively low densities, in the range 1-3 10^{10} cm^{-3}.

4. Hydrodynamic modelling

We have measured approximate loop sizes and inclination angles by manually tracing loop structures and estimating the inclination angles between the loop plane and the local vertical direction. We adopted the inclination angles that provide the most symmetrical curve in the loop plane. The procedure does not provide unique results, but gives approximate loop sizes. For example, for the central part of the arcade, we have estimated that loop 3 (cf. Fig. 8) has, with an inclination angle of 35 degrees, a length of 80 Mm and a maximum height of 22 Mm. The distance between the estimated footpoints is 58 Mm. The TRACE 195 Å images suggest loop widths of 3-4 TRACE pixels, i.e. of the order of 2", however sub-resolution structures can obviously be present.

We used the numerical code HYDRAD (Bradshaw & Mason 2003; Bradshaw et al. 2004) to perform the simulations. The aim of the simulations was to establish whether flows of the observed velocities at particular temperatures could reasonably be expected; for example, downflows $>$ 100 km s^{-1} at temperatures of order 10^5 K. The latest version (v.3) of HYDRAD comprises a two-fluid description of the plasma, though in the current work we preferentially heat the electrons

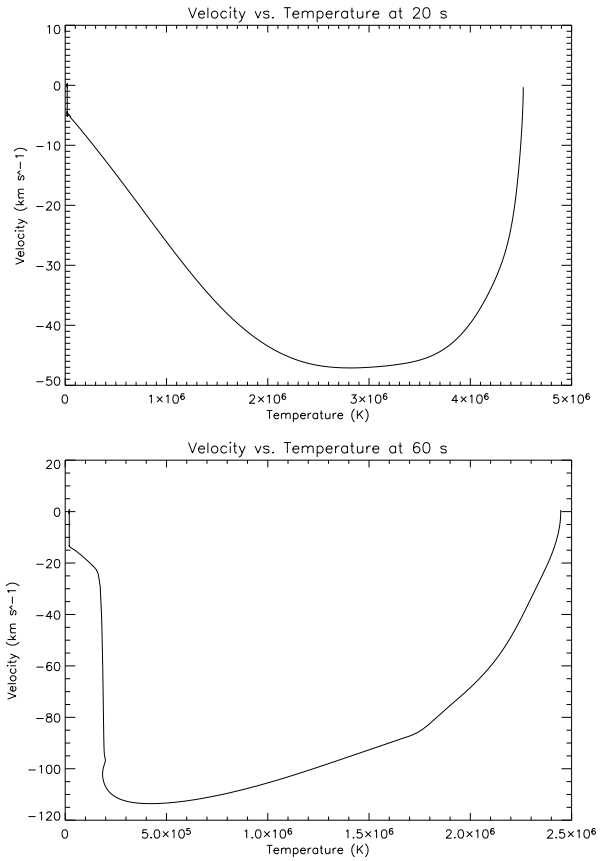

Figure 12. Results from the HYDRAD simulation, showing plasma velocities vs. temperatures at 20 and 60s. Only the left half of the loop is shown. Negative velocities correspond to down-flows.

and the temperature we refer to is the electron temperature. Of course, the question of electron vs. ion heating in solar flares is an important subject, which we will address in future work.

The dynamical behaviour evident in the observational data suggests heating taking place in the upper regions of the loops. For the purpose of the simulations we locate it at the apex, with the following properties: duration = 10 s; characteristic scale-length = 4000 km; rate of energy input = 1.0 erg cm^{-3} s^{-1}. The envelope of the heating profile is such that it is ramped up (exponentially, with an e-folding time-scale of 0.1 s) from 0.0 to 1.0 erg cm^{-3} s^{-1} in the first second; remains constant at 1.0 erg cm^{-3} s^{-1} for 8 s; and decays (again, exponentially, with an e-folding time-scale of 0.1 s) from 1.0 to 0.0 erg cm^{-3} s^{-1} in the final second of heating.

The results of these simulations are generally consistent with the observed properties of the loops in the arcade. Fig. 12 shows as an example two snaphots of velocities vs. temperatures at 20 and 60s. The top temperature reached in the loop is just short of 7 MK. At 20s the bulk of the downflows are at coronal temperatures, while at 60s they occur at transition region temperatures. This is clearly what is observed. The largest downflows are observed by CDS in O V. The absolute values of the flows are also in overall agreement with the observations, considering the projection effects and the low spatial-temporal resolution of CDS. Obviously, detailed forward modelling will be needed in order to fully tie in the hydrodynamics and the energetics with the observations. However this is beyond the scope of this paper.

5. Discussion and Conclusion

The set of observations that we analysed in this paper relate to the late phase of a long duration event (LDE) oberved on October 28 2003, one hour and half after the onset of the X17 flare. A well developed post-flare arcade is observed. We measure the flows over a large temperature range with CDS. The central area of the arcade, connecting the R1 and R2 ribbons, has features that are consistent with the 'standard' magneto-hydrodynamical models. The observed pattern of up-flows and down-flows is in agreement with models that explain the creation of flare loops by chromospheric evaporation driven by reconnection, with the exception that the main flows appear to be mostly concentrated on one side of the arcade. Slow chromospheric evaporation fills loops which then reconnect and become bright. The material in the loops is rapidly cooling by conduction and radiative losses (see, e.g., Schmieder et al. 1995; Bradshaw and Cargill 2005), and plasma at all temperatures is observed. The heating is quickly switched off and near the legs of the loops the cooling is dominated by radiation and becomes catastrophic. The plasma is falling down with near free fall velocities. The plasma velocity at hot temperatures (Fe XIX, 8 10^6 K) is nearly zero, but more than 70 km/s at transition region temperatures (O V, 10^5 K), and estimated to be larger than 100 km/s in Hα (10^4 K). Over the ribbons it is difficult to derive the Hα Doppler-shifts because the ribbons overlay sunspots. Complex non-LTE modelling with an appropriate sunspot atmosphere would be needed to obtain accurate values of Doppler-shifts.

The observed velocities are consistent with those predicted with 1-D hydrodynamical models (see Antiochos and Krall 1979, Doschek et al. 1982, but also Bradshaw et al. 2004 for a discussion on the

effects of time-dependent ionization). We ran a HYDRAD simulation to show that the properties of the observed flare loops are generally consistent with a short (seconds) heating near the loop top, followed by catastrophic cooling.

A puzzling aspect relates to the upflows that must be present to replenish the observed loops. CDS did observe upflows in O V and Mg X all along a thin region just outside ribbon R1, and co-spatial with a region of very low emission in the TRACE 195 Å band. The TRACE sequence of images show the persistence of this region during the entire gradual phase, hence it is likely that these 'gentle' upflows persisted all the time in the outer edges of the ribbon, as the two main ribbons separated. Note that projection effects would have actually favored observation of upflows near the other ribbon R2. However, the presence of smaller up-flows outside R2 cannot be ruled out.

Unlike the flare described by Czaykowska et al. (1999), in our case we did not observe significant up-flows in the hotter lines (Fe XIX).

A puzzling aspect of these observations is related to the area R3, located between the two ribbons R1 and R3. Unfortunately, CDS only observed the top part of R3, so we are unable to provide more details on this interesting part of this complex flare.

Acknowledgements

GDZ and HEM acknowledge support from PPARC.

SJB is supported by a PPARC Post-Doctoral Fellowship.

SOHO is a project of international collaboration between ESA and NASA.

We acknowledge the use of the TRACE, SOHO on-line databases.

We warmly thank the CDS team for their support in obtaining the observations, and the Kanzelhohe and Ondrejov observatories for providing ground-based data.

References

Antiochos, S. K., & Sturrock, P. A. 1978, ApJ, 220, 1137
Antiochos, S. K., & Krall, K. R. 1979, ApJ, 229, 788
Asai A., Masuda S., Yokoyama T et al., 2002, ApJ, 578, L91
Berlicki A., Heinzel P., Schmieder B., Mein P., Mein N. 2005, A&A, 430, 679
Bradshaw S. J & Mason H.E., 2003, A&A, 407, 1127
Bradshaw S. J., Del Zanna G. & Mason H.E., 2004, A&A, 425, 287
Bradshaw, S. J. and Cargill, P. J., 2005, A&A 437, 311-317
Czaykowska A.B., de Pontieu B., Alexander D., Rank G. 1999, ApJL, 521, L75

Del Zanna, G., Gibson, S. E., Mason, H. E., Pike, C. D., & Mandrini, C. H. 2002, Advances in Space Research, 30, 551
Del Zanna G., Berlicki A., Schmieder B., Mason H.E., 2006, Sol. Phys., 234,95
Doschek, G. A., Boris, J. P., Cheng, C. C., Mariska, J. T., & Oran, E. S. 1982, ApJ, 258, 373
Fletcher L. and Hudson H. 2001, Sol. Phys., 204, 69
Forbes, T. G., & Malherbe, J. M. 1986, ApJL, 302, L67
Forbes, T. G., & Acton, L. W. 1996, ApJ, 459, 330
Harra, L. K., Démoulin, P., Mandrini, C. H., Matthews, S. A., van Driel-Gesztelyi, L., Culhane, J. L., & Fletcher, L. 2005, A&A, 438, 1099
Kamio S., Kurokawa H., Ishii T.T., 2003, Sol. Phys, 215, 127
Kopp, R. A., & Pneuman, G. W. 1976, Sol. Phys., 50, 85
Kopp, R. A., & Poletto, G. 1984, Sol. Phys., 93, 351
Li H., Li J.P., Fang C., Schmieder B., Berlicki A., Du Q.S. 2006, Chinese J. Astron. and Astrophys., 15, 6, 645
Li H., Berlicki A., Schmieder B., 2005, A&A, 438,325
Régnier S. and Fleck B., 2004, ESA SP575, 519
Schmieder B., Heinzel P., Wiik J.E., Lemen J., Anwar B., Kotrc P., Hiei E., 1995, Sol. Phys., 156, 337
Schmieder B., Heinzel P., van Driel-Gesztelyi L., Lemen J.R., 1996, Sol. Phys., 165, 303
Schmieder B., Mandrini C.H., Démoulin P., Pariat E., Berlicki A., DeLuca E. 2006, Advances in Space Research, in press
Zhang H.Q., Bao X.M., Zhang Y., Liu J.H., Bao S.D., Deng Y.Y. et al. 2003, Chin.J.Astron.Astrophys. 3, 491
Wiik J.E., Schmieder B., Heinzel P., Roudier T., 1996, Sol. Phys., 166, 89